

# Large Lyman- $\alpha$ opacity fluctuations and low CMB $\tau$ in models of late reionization with large islands of neutral hydrogen extending to $z < 5.5$

Girish Kulkarni<sup>1,2,6\*</sup>, Laura C. Keating<sup>3</sup>, Martin G. Haehnelt<sup>1,2</sup>, Sarah E. I. Bosman<sup>4</sup>, Ewald Puchwein<sup>1,2,7</sup>, Jonathan Chardin<sup>5</sup> and Dominique Aubert<sup>5</sup>

<sup>1</sup>*Institute of Astronomy, University of Cambridge, Madingley Road, Cambridge CB3 0HA, UK*

<sup>2</sup>*Kavli Institute of Cosmology, University of Cambridge, Madingley Road, Cambridge CB3 0HA, UK*

<sup>3</sup>*Canadian Institute for Theoretical Astrophysics, 60 St. George Street, University of Toronto, ON M5S 3H8, Canada*

<sup>4</sup>*Department of Physics and Astronomy, University College London, London WC1E 6BT, UK*

<sup>5</sup>*Observatoire Astronomique de Strasbourg, 11 rue de l'Université, 67000 Strasbourg, France*

<sup>6</sup>*Department of Theoretical Physics, Tata Institute of Fundamental Research, Homi Bhabha Road, Mumbai 400005, India*

<sup>7</sup>*Leibniz-Institut für Astrophysik Potsdam (AIP), An der Sternwarte 16, D-14482 Potsdam, Germany*

Accepted —. Received —; in original form —

## ABSTRACT

High-redshift QSO spectra show large spatial fluctuations in the Ly $\alpha$  opacity of the intergalactic medium on surprisingly large scales at  $z \gtrsim 5.5$ . We present a radiative transfer simulation of cosmic reionization driven by galaxies that reproduces this large scatter and the rapid evolution of the Ly $\alpha$  opacity distribution at  $5 < z < 6$ . The simulation also reproduces the low Thomson scattering optical depth reported by the latest CMB measurement and is consistent with the observed short near-zones and strong red damping wings in the highest-redshift QSOs. It also matches the rapid disappearance of observed Ly $\alpha$  emission by galaxies at  $z \gtrsim 6$ . Reionization is complete at  $z = 5.3$  in our model, and 50% of the volume of the Universe is ionized at  $z = 7$ . Agreement with the Ly $\alpha$  forest data in such a late reionization model requires a rapid evolution of the ionizing emissivity of galaxies that peaks at  $z \sim 6.8$ . The late end of reionization results in a large scatter in the photoionisation rate and the neutral hydrogen fraction at redshifts as low as  $z \lesssim 5.5$  with large residual neutral ‘islands’ that can produce very long Gunn-Peterson troughs resembling those seen in the data.

**Key words:** dark ages – reionization, first stars – intergalactic medium – radiative transfer – galaxies: high-redshift – quasars: absorption lines

## 1 INTRODUCTION

The effective optical depth ( $\tau_{\text{eff}}$ ) of Lyman- $\alpha$  (Ly $\alpha$ ) absorption in QSO spectra at redshift  $z \gtrsim 5$  is observed to exhibit large spatial fluctuations (Fan et al. 2006; Willott et al. 2007; Becker et al. 2015; Barnett et al. 2017; Tang et al. 2017; Bosman et al. 2018; Eilers et al. 2018). Becker et al. (2015) showed that the dispersion in  $\tau_{\text{eff}}$  at these redshifts is significantly larger than that expected from density fluctuations alone (Lidz et al. 2006, 2007; Mesinger 2010). Although this suggests that the observed Ly $\alpha$  data are probing a fluctuating UV background due to patchy reionization, Becker et al. (2015) found that the scatter in  $\tau_{\text{eff}}$  is also greater than that in models with a fluctuating UV background with a spatially uniform mean free path of ionizing photons.

Using a semi-numerical reionization model, Davies & Furlanetto (2016) showed that fluctuations in the mean free path due to

spatial variation in the photoionisation rate and gas density can explain the observed distribution of  $\tau_{\text{eff}}$  at  $z = 5.6$ , albeit with a rather short mean free path that decreases rapidly with distance from (bright) ionizing sources and that is in the mean a factor of 3.6 smaller than that expected from an extrapolation of measurements at  $z = 4.56\text{--}5.16$  (Worseck et al. 2014). The model by Davies & Furlanetto (2016) also does not address the rather rapid evolution of the Ly $\alpha$  opacity distribution at  $5 < z < 6$ . Chardin et al. (2015, 2017) presented a model where the observed large  $\tau_{\text{eff}}$  fluctuations arise due to fluctuations in a UV background with a significant contribution from rare, bright sources such as quasars that have a mean separation greater than the mean free path. Despite the resulting large fluctuations of the photoionisation rate the “rare-source model” of Chardin et al. (2015) struggled, however, to reproduce the long (up to 110 cMpc/h) and dark ( $\tau_{\text{eff}} \gtrsim 7$ ) Ly $\alpha$  absorption troughs seen down to  $z \sim 5.5$  (Becker et al. 2015) unless the space density of intermediate-brightness quasars is higher than that inferred from QSO surveys (Kulkarni et al. 2018) by a factor 3–

\* Email: kulkarni@theory.tifr.res.in

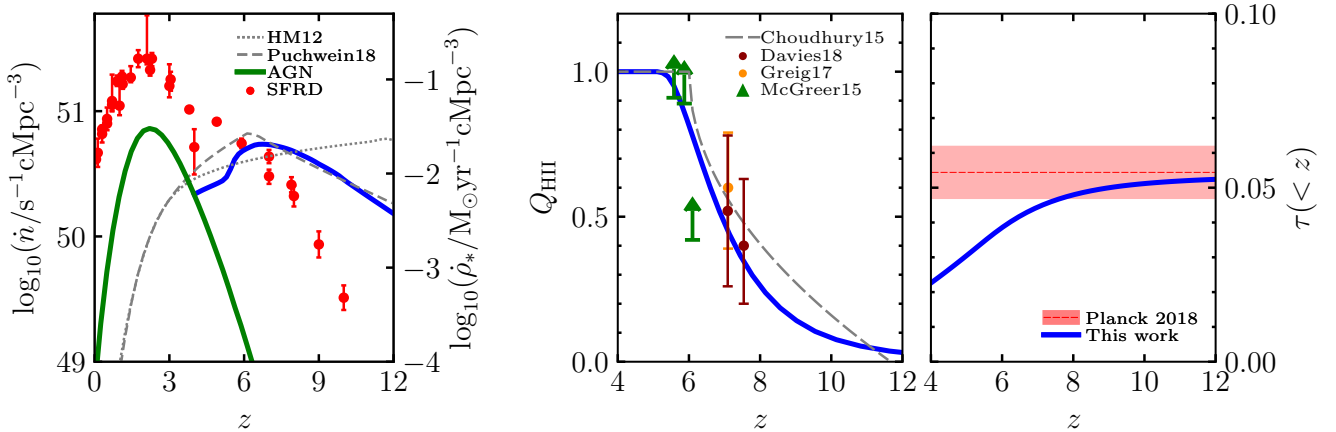


**Figure 1.** The comoving ionizing emissivity evolution in our simulation is shown by the blue curve in the left panel. Red data points show cosmic star formation rate density estimates at  $z = 9$  and  $10$  from Oesch et al. (2014) and Oesch et al. (2018) and at lower redshifts from the compilation by Madau & Dickinson (2014). The green curve shows the comoving ionizing emissivity from AGN brighter than  $M_{1450} = -21$  from Kulkarni et al. (2018). The ionizing emissivity due to galaxies in the models by Haardt & Madau (2012) and Puchwein et al. (2018) are shown by the grey dotted and dashed curves, respectively. The middle panel shows the volume-averaged ionized hydrogen fraction, which does not reach  $Q_{\text{HII}} = 1$  before  $z = 5.3$ . Also shown are constraints on  $Q_{\text{HII}}$  by Greig et al. (2017) and Davies et al. (2018a) from the red damping wings and short near-zones in the two highest redshift QSOs known at  $z = 7.1$  and  $7.5$  (with corresponding 68% uncertainties), and lower limits on the ionized hydrogen fraction from McGreer et al. (2015) derived from dark pixels in Ly $\alpha$  and Ly $\beta$  forests. The grey curve shows the evolution of  $Q_{\text{HII}}$  from the ‘Very Late’ reionization model that Choudhury et al. (2015) have shown to be consistent with the rapid disappearance of the Ly $\alpha$  emission of high-redshift galaxies. The right panel shows the electron scattering optical depth  $\tau$ , together with the Planck Collaboration VI (2018) measurement of  $\tau = 0.0544 \pm 0.0073$ .

10 (Chardin et al. 2017). The required large contribution of QSOs to the ionizing emissivity at 1 Ry appears also to be in conflict with the observed He II opacity and measurements of the temperature of the IGM (D’Aloisio et al. 2017; Puchwein et al. 2018) unless unlike normal QSOs the rare ionizing sources have little emission at energies larger than 1 Ry. Another explanation for the large fluctuations in  $\tau_{\text{eff}}$  was proposed by D’Aloisio et al. (2015), who argued that spatial variation in gas temperature can lead to the observed scatter in  $\tau_{\text{eff}}$  due to the temperature dependence of the recombination rate, albeit with a reionization history that is more extended than suggested by recent CMB and Ly $\alpha$  absorption and emission data (see Keating et al. 2018 for a discussion).

While efforts are underway to observationally determine which of these models describes the origin of the  $\tau_{\text{eff}}$  fluctuations (Becker et al. 2018; Davies et al. 2018b), it is clearly necessary to self-consistently model spatial variation in the UV background, the mean free path of ionizing photons, and the gas temperature in radiative transfer simulations of reionization. In this Letter, we present results from such a simulation that allows us to probe scales larger than the rapidly increasing mean free path during the overlap of H II regions. This has become possible by pushing our simulations to  $2048^3$  particles/cells with a box size of  $160 \text{ Mpc}/h$  that allow us to sample a large enough cosmological volume at sufficient resolution while enabling us to avoid several simplifying assumptions made in the models described above. After deriving the spatial distribution of the neutral hydrogen fraction, the photoionization rate, and the gas temperature, we investigate the distribution of  $\tau_{\text{eff}}$  and compare it to data. We present the details of our simulation in Section 2. Section 3 discusses the  $\tau_{\text{eff}}$  fluctuations in our model. Our  $\Lambda\text{CDM}$  cosmological model has  $\Omega_b = 0.0482$ ,  $\Omega_m = 0.308$ ,  $\Omega_\Lambda = 0.692$ ,  $h = 0.678$ ,  $n_s = 0.961$ ,  $\sigma_8 = 0.829$ , and  $Y_{\text{He}} = 0.24$  (Planck Collaboration XVI 2014).

## 2 SIMULATION SET-UP AND CALIBRATION

We perform single-frequency cosmological radiative transfer using the ATON code (Aubert & Teyssier 2008, 2010), following an approach similar to Chardin et al. (2015) and Keating et al. (2018). Cosmological density fields obtained from hydrodynamical simulations are post-processed by ATON.

Our cosmological hydrodynamical simulation was performed using the P-GADGET-3 code, which is derived from the GADGET-2 code (Springel et al. 2001; Springel 2005). We used a box size of  $160 \text{ cMpc}/h$  with  $2048^3$  gas and dark matter particles with a dark matter particle mass of  $M_{\text{dm}} = 3.44 \times 10^7 M_\odot/h$  and gas particle mass of  $M_{\text{gas}} = 6.38 \times 10^6 M_\odot/h$ . The initial conditions are identical to those of the  $160\text{--}2048$  simulation from the Sherwood simulation suite (Bolton et al. 2017). These initial conditions were evolved from  $z = 99$  to  $z = 4$ . We saved 38 snapshots at 40 Myr intervals. In order to speed up the simulation, we used the QUICK\_LYALPHA option in P-GADGET-3 to convert gas particles with temperature less than  $10^5 \text{ K}$  and overdensity of more than a thousand to star particles (Viel et al. 2004). This approximation does not affect the reionization process as the mean free path of ionizing photons is determined by self-shielded regions with a typical overdensity of  $\Delta = 10\text{--}100$  (Pawlik et al. 2009; Chardin et al. 2018). We grid the gas density on a cartesian grid with the number of grid cells equal to the number of SPH particles, yielding a grid resolution of  $78.125 \text{ ckpc}/h$ . ATON is then used to perform radiative transfer in post-processing. ATON solves the radiative transfer equation by using a moment-based description with the M1 approximation for the Eddington tensor (Gnedin & Abel 2001; Aubert & Teyssier 2008) and self-consistently derives the fraction of ionized hydrogen and the gas temperature on the grid. The adiabatic cooling of gas due to cosmic expansion is accounted for. The hydrodynamic response of the gas due to the changes in temperature is neglected. However, we do not expect this to seriously affect the

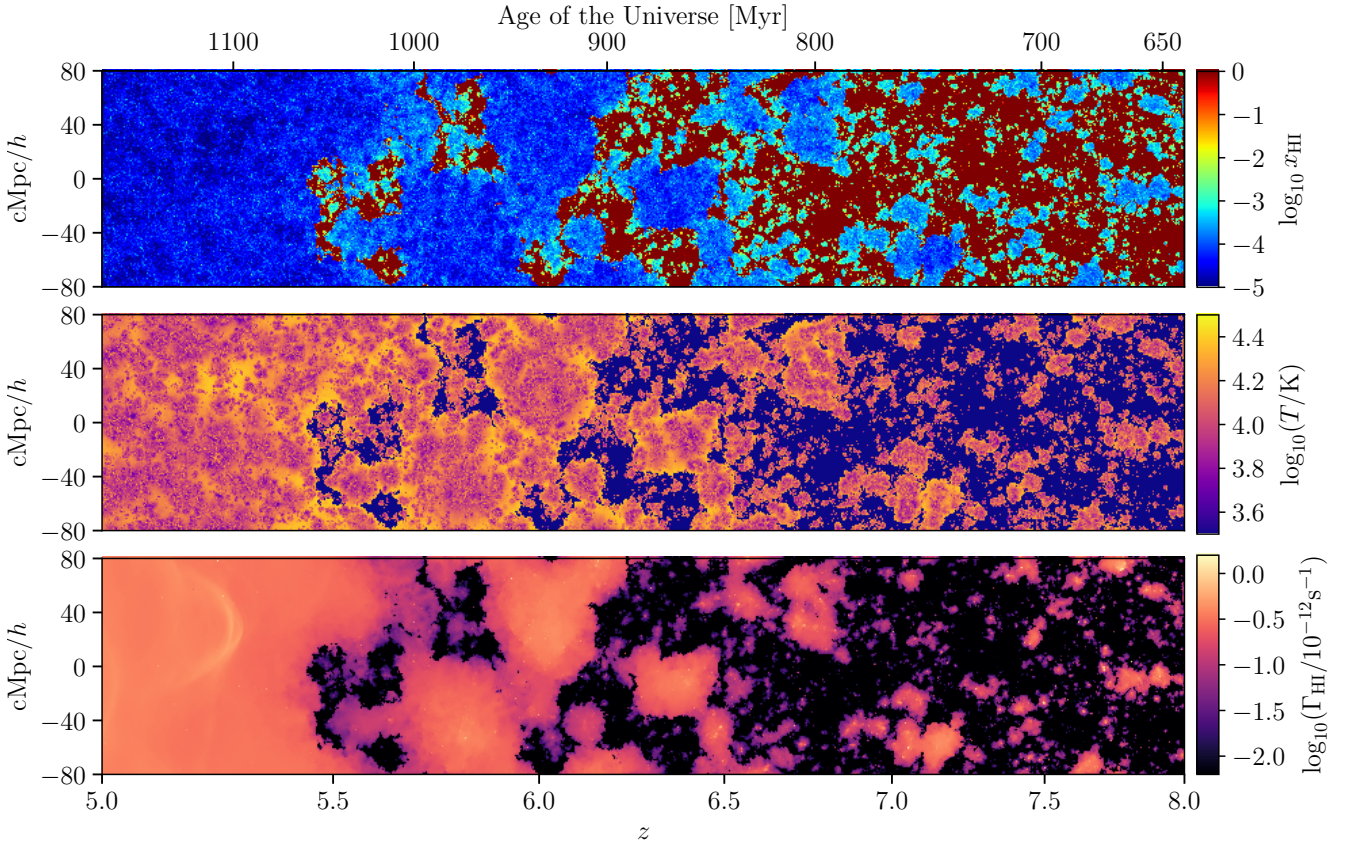


**Figure 2.** Evolution of the neutral hydrogen fraction (top panel), gas temperature (middle panel), and the hydrogen photoionization rate (bottom panel) from  $z = 8$  to 5 in the simulation.

results, as the pressure smoothing scale at redshifts  $z > 5$  for our chosen UV background is less than 100 ckpc/h (Kulkarni et al. 2015; Oñorbe et al. 2017), approximately equal to the cell size of our grid. Ionizing sources are placed at the centres of mass of haloes with masses above  $10^9 M_{\odot}/h$ .

We assume that the ionizing luminosity of a source,  $\dot{N}_{\gamma}$ , is proportional to its halo mass and require that the total volume emissivity  $\dot{n} = \sum \dot{N}_{\gamma}/V_{\text{box}}$ , where  $V_{\text{box}}$  is the box volume, matches a pre-selected emissivity evolution (cf. Chardin et al. 2015). Our chosen emissivity, shown in the left panel of Figure 1, peaks at redshift  $z \sim 6.8$  and drops towards higher redshifts somewhat more slowly than current estimates of the evolution of the cosmic star formation rate density. This is strikingly different from the evolution adopted by Chardin et al. (2015) and Keating et al. (2018), in which the emissivity at  $z > 7$  is much higher. The emissivity assumed here drops by a factor of two between  $z = 6.8$  and  $z = 4$ . As we discuss below, this decrease at  $z < 6.8$  allows us to reproduce the observed mean Ly $\alpha$  transmission at these redshifts, while the decrease in the emissivity towards higher redshift at  $z > 6.8$  results in a rather late reionization. Note that the emissivity model required to match the Ly $\alpha$  forest opacity as well as the Planck Collaboration VI (2018) Thompson scattering optical depth is similar to the fiducial model for the ionizing emissivity of galaxies in Puchwein et al. (2018). As in the Puchwein et al. (2018) model, the difference in the evolutionary trends of the emissivity and the cosmic star formation rate density (Figure 1) can be attributed to the evolution of the escape fraction of ionizing photons from galaxies, possibly due to changes in morphology, stellar populations, and dust con-

tent of these galaxies (Rosdahl et al. 2018; Trebitsch et al. 2017; Kimm et al. 2017; Paardekooper et al. 2015; Kimm & Cen 2014; Yajima et al. 2011). We use a single photon frequency to reduce the computational cost and assume that all sources have a blackbody spectrum with  $T = 70,000$  K (Keating et al. 2018). This yields an average photon energy of 23.83 eV in the optically thick limit. We have varied these assumptions and found our results to be robust. We will discuss more details in future work.

### 3 LARGE Ly $\alpha$ OPACITY FLUCTUATIONS

Figure 1 shows the evolution of the volume-averaged ionized hydrogen fraction  $Q_{\text{HII}}$ . Reionization is considerably late in our simulation compared to most models in the literature (e.g., Haardt & Madau 2012), and is comparable to the ‘Very Late’ model shown by Choudhury et al. (2015) to be consistent with the rapid disappearance of Ly $\alpha$  emission of high-redshift galaxies. Half of the cosmic volume is reionized at  $z = 7.0$ . The duration of reionization, as quantified by the difference in the redshifts at which 5% and 95% cosmic volume is reionized,  $\Delta z \equiv z_{5\%} - z_{95\%}$ , is 3.89. Reionization is complete at  $z = 5.3$ . This evolution is also in excellent agreement with the determination of  $Q_{\text{HII}}$  at  $z = 7.1$  and 7.5 by Davies et al. (2018a) and at  $z = 7.1$  by Greig et al. (2017) from the red damping wing and the short near-zones in the two highest redshift QSOs known. Figure 1 also shows the electron scattering optical depth in our model,  $\tau_{\text{CMB}} = 0.054$ , in excellent agreement with the most recent determination of  $\tau_{\text{CMB}} = 0.0544 \pm 0.0073$  from Planck Collaboration VI (2018). Note that following Planck

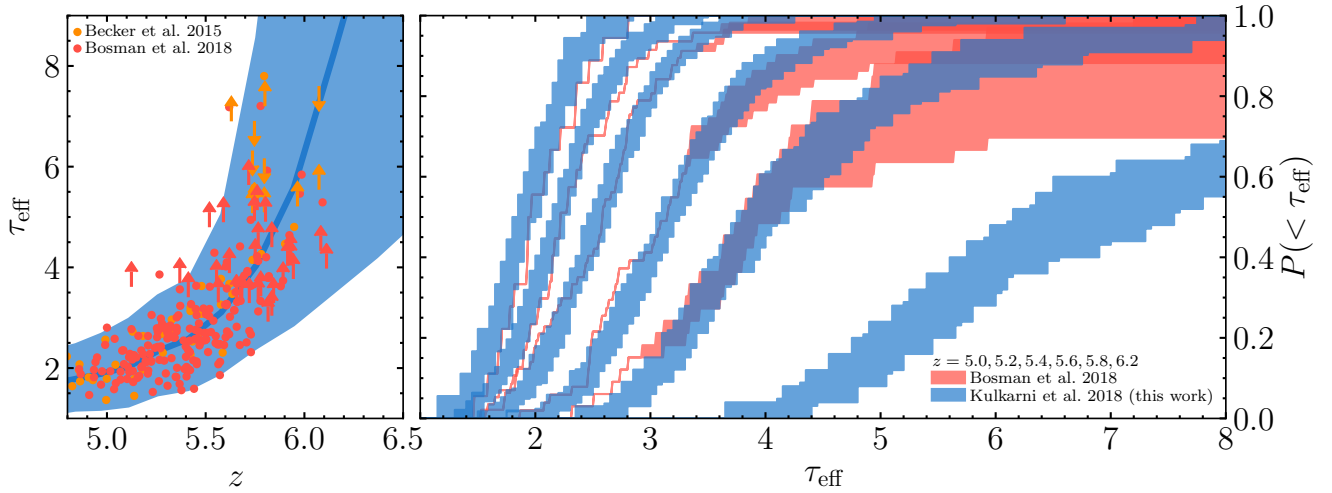


**Figure 3.** The left panel compares the evolution of the effective Ly $\alpha$  optical depth  $\tau_{\text{eff}}$  (measured over 50 cMpc/h) in the simulation with measurements by Becker et al. (2011) and Bosman et al. (2018). Non-detections are shown as lower limits. Upper limits in the measurements by Becker et al. (2011) indicate sightlines that do not have a formal detection but show individual transmission peaks. The solid curve shows the mean  $\tau_{\text{eff}}$  evolution in the simulation, with the shaded region indicating the central 98% extent. The right panel shows in blue the 68% scatter around the median cumulative distribution functions of  $\tau_{\text{eff}}$  of the simulated spectra at  $z = 5.0, 5.2, 5.4, 5.6, 5.8,$  and  $6.2$  (left to right). Also shown are the optimistic and pessimistic bounds measured by Bosman et al. (2018) at  $z \leq 5.8$ .

Collaboration VI 2018, we assume here that He II reionizes instantaneously at  $z = 3.5$ .

Figure 2 shows the neutral hydrogen fraction  $x_{\text{HI}}$ , gas temperature  $T$ , and the hydrogen photoionization rate  $\Gamma_{\text{HI}}$  from  $z = 5$  to 8. These lightcones nicely illustrate the patchy and delayed nature of reionization in our simulation, with ‘islands’ of neutral hydrogen several tens of megaparsecs in length persisting down to  $z < 5.5$ . Large coherent spatial variation of the neutral fraction are seen at even lower redshifts ( $z \sim 5$ ). These are accompanied by large-scale, coherent fluctuations (a factor of 3–4 at  $z < 5.5$ ) in the gas temperature that persist all the way down to  $z = 4$  (cf. Keating et al. 2018). Note that the photoionisation rate is significantly reduced in the vicinity of the remaining neutral islands likely due to a combination of these regions only being recently ionized and having a reduced mean free path for photons arriving from the direction of the neutral islands. Note further that the last neutral islands to be reionized attain the highest temperatures and switch from exhibiting the largest effective optical depth to exhibiting the lowest effective optical depth at a given redshift very quickly.

Observations traditionally quantify effective optical depths over spectral chunks corresponding to 50 cMpc/h. At  $z = 5.8$ , this corresponds to  $\Delta t \sim 35$  Myr. As seen in Figure 2, the IGM evolves rapidly over this time scale at these redshifts. To incorporate this rapid evolution in our simulated spectra, we interpolate lines of sight in time between different snapshots. Figure 3 shows the resultant evolution of  $\tau_{\text{eff}}$  in our model in comparison with measurements from Bosman et al. (2018) and Becker et al. (2015). Our simulated spectra match the data very well down to  $z = 4.9$ . The late end of reionization and the persistence of large neutral hydrogen islands down to  $z < 5.5$  result in sightlines that still have  $\tau_{\text{eff}} > 8$  at  $z = 5.7$ . Figure 3 also shows the cumulative distribution function of  $\tau_{\text{eff}}$  in six redshift bins from  $z = 5$  to 5.8 and at  $z = 6.2$ . At  $z = 5$ –5.8, we compare our results with the measurements by Bosman et al. (2018) who present their results as ‘optimistic’ and ‘pessimistic’ limits on the distribution. Lower

limits on  $\tau_{\text{eff}}$  are treated as measurements in the optimistic case, whereas these are assumed to have values greater than  $\tau_{\text{eff}} = 8$  in the pessimistic case. When comparing the simulation with data, we draw 50 samples with the same size and redshift distribution as that of the data in Bosman et al. (2018) and show the 68% scatter in Figure 3. At  $z = 6.2$ , where no measurements are available yet, we used a sample size of 25. The  $\tau_{\text{eff}}$  values reported by Eilers et al. (2018) are systematically higher than those measured by Bosman et al. (2018), but it is certainly possible to match the Eilers et al. (2018) data if we delay reionization in our model further. We also note that increasing the spatial resolution does not change our results, although for a factor-of-2 higher resolution we find that a small enhancement ( $\sim 10\%$ ) in the emissivity is required as more high-density absorbers are resolved. Similarly, changing the photon energy in our simulation does not affect the opacity fluctuations. Since the simulation is calibrated to the mean Ly $\alpha$  transmission, a change in the photon energy only marginally changes the ionization fraction and the required ionizing photon emissivity without altering the opacity distribution.

## 4 DISCUSSION AND CONCLUSIONS

We have presented a radiative transfer simulation of cosmic reionization by galaxies that closely agrees with the measurements of the effective Ly $\alpha$  opacity of the intergalactic medium at  $z = 5$ –6. Our reionization history also agrees very well with the electron scattering optical depth measurements from CMB experiments, as well as constraints on the ionization state of the IGM from QSO near-zones at  $z \sim 7$  and the rapid disappearance of Ly $\alpha$  emission from high-redshift galaxies. This very good agreement with a wide range of data is owed to reionization occurring rather late in the model with a rapid evolution in ionizing emissivity that is peaked at  $z \sim 6.8$  suggesting that the contribution of galaxies to the ionizing emissivity at  $z \lesssim 4$  is small. The reionization history in this model results in a broad scatter in the neutral hydrogen fraction and large neutral

hydrogen ‘islands’ persisting to redshifts as low as  $z \lesssim 5.5$ . As we will discuss in future work, these large late remaining neutral islands can result in long Gunn-Peterson troughs resembling those seen in the data. The simulation also shows large spatially coherent fluctuations of the temperature-density relation that persist down to  $z < 5$ . Unlike other proposed models, our modelling solves the mystery of the large scatter of the Ly $\alpha$  opacity on surprisingly large scales without requiring ionizing sources or properties of the IGM in tension with current observations and/or theoretical expectations. Published Ly $\alpha$  data already now provides very tight constraints on the ionization and thermal history of the IGM at  $z \leq 6$ . With further improved Ly $\alpha$  absorption/emission data and by adding information from Ly $\beta$  and metal absorption data it should soon be possible to fully map out the exact history of the second half ( $Q > 0.5$ ) of cosmic reionization or more.

## ACKNOWLEDGEMENTS

This work used the Cambridge Service for Data Driven Discovery (CSD3) operated by the University of Cambridge ([www.csd3.cam.ac.uk](http://www.csd3.cam.ac.uk)), provided by Dell EMC and Intel using Tier-2 funding from the Engineering and Physical Sciences Research Council (capital grant EP/P020259/1), and DiRAC funding from the Science and Technology Facilities Council ([www.dirac.ac.uk](http://www.dirac.ac.uk)). This work further used the COSMA Data Centric system operated Durham University on behalf of the STFC DiRAC HPC Facility. This equipment was funded by a BIS National E-infrastructure capital grant ST/K00042X/1, DiRAC Operations grant ST/K003267/1 and Durham University. DiRAC is part of the National E-Infrastructure. We thank Joseph Hennawi and Anna-Christina Eilers for data and discussions. We acknowledge support from ERC Advanced Grant 320596 ‘Emergence’.

## REFERENCES

- Aubert D., Teyssier R., 2008, *MNRAS*, **387**, 295  
Aubert D., Teyssier R., 2010, *ApJ*, **724**, 244  
Barnett R., Warren S. J., Becker G. D., Mortlock D. J., Hewett P. C., McMahon R. G., Simpson C., Venemans B. P., 2017, *A&A*, **601**, A16  
Becker G. D., Bolton J. S., Haehnelt M. G., Sargent W. L. W., 2011, *MNRAS*, **410**, 1096  
Becker G. D., Bolton J. S., Madau P., Pettini M., Ryan-Weber E. V., Venemans B. P., 2015, *MNRAS*, **447**, 3402  
Becker G. D., Davies F. B., Furlanetto S. R., Malkan M. A., Boera E., Douglas C., 2018, *ApJ*, **863**, 92  
Bolton J. S., Puchwein E., Sijacki D., Haehnelt M. G., Kim T.-S., Meiksin A., Regan J. A., Viel M., 2017, *MNRAS*, **464**, 897  
Bosman S. E. I., Fan X., Jiang L., Reed S., Matsuoka Y., Becker G., Haehnelt M., 2018, *MNRAS*,  
Chardin J., Haehnelt M. G., Aubert D., Puchwein E., 2015, *MNRAS*, **453**, 2943  
Chardin J., Puchwein E., Haehnelt M. G., 2017, *MNRAS*, **465**, 3429  
Chardin J., Kulkarni G., Haehnelt M. G., 2018, *MNRAS*, **478**, 1065  
Choudhury T. R., Puchwein E., Haehnelt M. G., Bolton J. S., 2015, *MNRAS*, **452**, 261  
D’Aloisio A., McQuinn M., Trac H., 2015, *ApJ*, **813**, L38  
D’Aloisio A., Upton Sanderbeck P. R., McQuinn M., Trac H., Shapiro P. R., 2017, *MNRAS*, **468**, 4691  
Davies F. B., Furlanetto S. R., 2016, *MNRAS*, **460**, 1328  
Davies F. B., et al., 2018a, arXiv:1802.06066 [astro-ph.CO]  
Davies F. B., Becker G. D., Furlanetto S. R., 2018b, *ApJ*, **860**, 155  
Eilers A.-C., Davies F. B., Hennawi J. F., 2018, *ApJ*, **864**, 53  
Fan X., et al., 2006, *AJ*, **132**, 117

- Gnedin N. Y., Abel T., 2001, *New Astron.*, **6**, 437  
Greig B., Mesinger A., Haiman Z., Simcoe R. A., 2017, *MNRAS*, **466**, 4239  
Haardt F., Madau P., 2012, *ApJ*, **746**, 125  
Keating L. C., Puchwein E., Haehnelt M. G., 2018, *MNRAS*, **477**, 5501  
Kimm T., Cen R., 2014, *ApJ*, **788**, 121  
Kimm T., Katz H., Haehnelt M., Rosdahl J., Devriendt J., Slyz A., 2017, *MNRAS*, **466**, 4826  
Kulkarni G., Hennawi J. F., Oñorbe J., Rorai A., Springel V., 2015, *ApJ*, **812**, 30  
Kulkarni G., Worseck G., Hennawi J. F., 2018, arXiv:1807.09774 [astro-ph.GA]  
Lidz A., Oh S. P., Furlanetto S. R., 2006, *ApJ*, **639**, L47  
Lidz A., McQuinn M., Zaldarriaga M., Hernquist L., Dutta S., 2007, *ApJ*, **670**, 39  
Madau P., Dickinson M., 2014, *ARA&A*, **52**, 415  
McGreer I. D., Mesinger A., D’Odorico V., 2015, *MNRAS*, **447**, 499  
Mesinger A., 2010, *MNRAS*, **407**, 1328  
Oñorbe J., Hennawi J. F., Lukić Z., 2017, *ApJ*, **837**, 106  
Oesch P. A., et al., 2014, *ApJ*, **786**, 108  
Oesch P. A., Bouwens R. J., Illingworth G. D., Labbé I., Stefanon M., 2018, *ApJ*, **855**, 105  
Paardekooper J.-P., Khochfar S., Dalla Vecchia C., 2015, *MNRAS*, **451**, 2544  
Pawlik A. H., Schaye J., van Scherpenzeel E., 2009, *MNRAS*, **394**, 1812  
Planck Collaboration VI 2018, arXiv:1807.06209 [astro-ph.CO]  
Planck Collaboration XVI 2014, *A&A*, **571**, A16  
Puchwein E., Haardt F., Haehnelt M. G., Madau P., 2018, arXiv:1801.04931 [astro-ph.GA]  
Rosdahl J., et al., 2018, *MNRAS*, **479**, 994  
Springel V., 2005, *MNRAS*, **364**, 1105  
Springel V., Yoshida N., White S. D. M., 2001, *New Astron.*, **6**, 79  
Tang J.-J., et al., 2017, *MNRAS*, **466**, 4568  
Trebitsch M., Blaizot J., Rosdahl J., Devriendt J., Slyz A., 2017, *MNRAS*, **470**, 224  
Viel M., Haehnelt M. G., Springel V., 2004, *MNRAS*, **354**, 684  
Willott C. J., et al., 2007, *AJ*, **134**, 2435  
Worseck G., et al., 2014, *MNRAS*, **445**, 1745  
Yajima H., Choi J.-H., Nagamine K., 2011, *MNRAS*, **412**, 411

This paper has been typeset from a  $\text{\TeX}/\text{\LaTeX}$  file prepared by the author.